Lab on a Chip

View Online
Dynamic Article Links

Cite this: DOI: 10.1039/c0lc00568a

www.rsc.org/loc

PAPER

A unified platform for optoelectrowetting and optoelectronic tweezers†

Justin K. Valley,* Shao NingPei, Arash Jamshidi, Hsan-Yin Hsu and Ming C. Wu

Received 6th November 2010, Accepted 10th January 2011
DOI: 10.1039/c0lc00568a

A platform capable of seamlessly unifying both optoelectrowetting and optoelectronic tweezers is presented. This enables the user to manipulate aqueous droplets (with electrowetting) as well as individual particles within those droplets (with dielectrophoresis). The device requires no photolithography and droplet/particle manipulation can occur continuously over the entire surface of the device. Droplet and 10 μm polystyrene particle speeds of up to 8 mm s^{-1} and 60 μm s^{-1}, respectively, are demonstrated. Particle concentration within, and subsequent splitting of, a droplet is performed resulting in average concentration efficiencies of 93%. Serial concentration is also demonstrated resulting in exponentially increasing particle concentrations and a 10× concentration increase. Finally, the platform is used to select a single cell out of a cohort and subsequently encapsulate it in its own aqueous droplet.

Introduction

The field of microfluidics and micro total analysis systems has seen tremendous growth in the last decade. While many had hoped for a large-scale commercialization of the technology by now, the killer application for these devices remains elusive.[1] The eventual products that manifest out of this research will likely incorporate a multitude of the features and phenomena (*e.g.* capillary action, electrophoresis, electroosmosis, electrowetting, dielectrophoresis, *etc.*) associated with the field. The integration of multiple techniques on-chip allows for a versatile and powerful microsystem for applications in the biological and chemical processing fields. In the context of this report, an interesting example involves the integration of *individual* droplet control (*i.e.* electrowetting-on-dielectric[2–4] (EWOD)) along with a manipulation technique for particles within the droplets. A successful device would enable a variety of applications ranging from on-chip sample concentration/purification to single particle encapsulation.

The concept of integrating individual droplet control along with a means of controlling the particles within those droplets is not new. In fact a variety of work exists attempting to merge these two techniques. Not surprisingly, all prior work utilizes EWOD as the means for droplet manipulation. However, the particle manipulation techniques are more diverse and include electrophoresis,[5] magnetophoresis,[6] dielectrophoresis (DEP),[7,8] and optoelectronic tweezers (OET) (also known as light-induced DEP (LiDEP)).[9] Of all the particle manipulation techniques listed, DEP (also OET) is likely the most versatile as it acts on any polarizable particle (even charge neutral ones) and the particle's response is intrinsically related it's unique impedance spectrum enabling a means for particle sorting and identification.

While all of this work takes great strides towards realizing an integrated droplet/particle manipulation system, each reported platform suffers from three distinct drawbacks. First, each reported system restricts particle movement to specific regions of the chip. This is essentially a constraint imposed by the fact that the electrodes required for droplet manipulation (EWOD) are geometrically different from those used for particle manipulation. Therefore, droplet and particle manipulation can only occur where EWOD-specific and particle-specific electrodes exist, respectively. This limits the number of particle manipulation sites and requires careful electrode layout for a given application. Secondly, all of these platforms require *relatively* complex fabrication. Namely, they require at least 1 lithographic step. This, once again, is due to the use of discrete patterned microelectrodes for droplet and particle manipulation. Finally, none of these devices enables full 2-dimensional *single* particle control (in fact, with the exception of the 1-dimensional single particle control afforded by Shah *et al.*, the other techniques can only move ensembles of particles).[9] For some applications, such as selective single particle encapsulation, the ability to select and move individual particles over an arbitrary path in the droplet is critical.

In this report, we aim to address these issues by presenting a platform that uses optoelectrowetting (OEW)[10–12] and OET[13] (chosen through a simple change in device bias) to enable droplet and particle control, respectively. This technique requires no lithographically defined microelectrodes, since electrodes are created using patterned light, and, as such, device fabrication

Berkeley Sensor and Actuator Center, Department of Electrical Engineering and Computer Science, University of California Berkeley, 497 Cory Hall, Berkeley, CA, 94720, USA. E-mail: valleyj@eecs.berkeley.edu; Fax: +1 510 643 5817; Tel: +1 510 642 1023

† Electronic supplementary information (ESI) available: Videos S1 and S2. See DOI: 10.1039/c0lc00568a

requires only planar deposition (no lithography). Additionally, since patterned light acts to define the electrodes, particle/droplet manipulation can occur anywhere on the surface of the device and full 2-dimensional single particle control is enabled.

Device operation

An understanding of how both OEW and OET can be achieved on the same device is depicted in Fig. 1. The actual device used is shown in Fig. 1a. Here a liquid droplet is sandwiched between a top, Teflon-coated indium–tin-oxide (ITO) electrode and a bottom ITO electrode coated with a photosensitive layer of a-Si:H, an insulating layer of Al_2O_3, and a Teflon layer.

An external bias is then applied between the two ITO electrodes. In the absence of incident light, the electric field primarily exists in the highly resistive a-Si:H layer. However, upon illumination, the conductivity of the a-Si:H layer increases dramatically and causes the electric field, in general, to drop across a combination of the dielectric (oxide and Teflon) and liquid layers. If the majority of the field drops across the dielectric layer, then the droplet will experience a net electromechanical force towards the illuminated region (*i.e.* OEW). However, if the majority of the field drops across the liquid layer, electric field gradients will exist in the liquid (due to the spatial localization of the light pattern) and exert dielectrophoretic forces on particles within the droplet (*i.e.* OET).

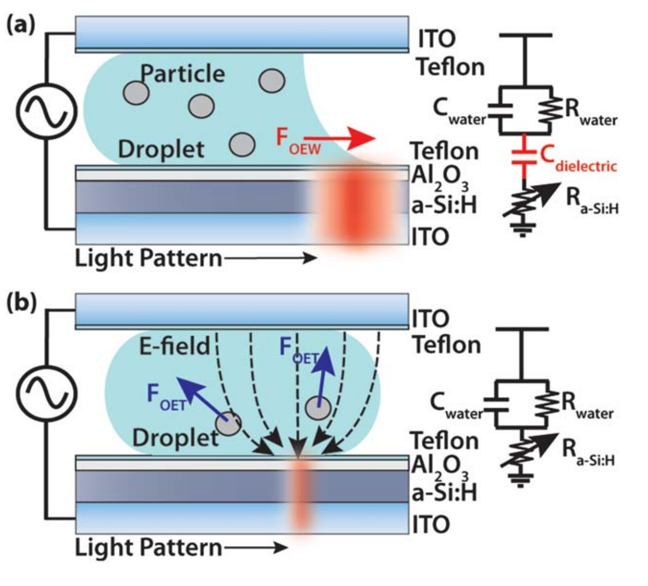

Fig. 1 Device schematic. (a) Diagram of the device operating in OEW modality (valid for frequencies, $f < 100$ kHz). Incident light interacts with the photoconductive a-Si:H layer and locally concentrates the electric field across a thin Al_2O_3 and Teflon dielectric layer ($C_{dielectric}$). This causes aqueous droplets in the vicinity to move towards the light pattern. Particles within the droplet are transported along with the droplet. (b) Diagram of the device operating in OET modality ($f > 100$ kHz). In this modality, the electrically insulating Al_2O_3 and Teflon layers are shorted out ($C_{dielectric}$) and the field is now concentrated in the liquid/droplet layer. Therefore, particles within the droplet experience a DEP force when in the vicinity of incident optical energy. In this regime, the device electrically looks identical to standard optoelectronic tweezers.

The question then becomes how one controls whether the field drops primarily across the dielectric or liquid layer. Since this is essentially just a question of which layer's impedance is larger, the answer is through the proper choice of the externally applied electrical frequency. This can be seen by comparing the equivalent device circuit diagrams of Fig. 1a and b. In Fig. 1a, a capacitor is present to model the effect of the dielectric layer. Below a critical frequency, the impedance of this capacitor will dominate over the liquid layer impedance. However, above this critical frequency, the impedance of the dielectric becomes negligible compared to the liquid resistance. Namely, the device goes from operating in the OEW regime to the OET regime. It should be noted that Fig. 1b looks electrically identical to the traditional OET device (*i.e.* optoelectronic tweezers[13]).

A simplified graphical depiction of the frequency dependence of the device is shown in Fig. 2a. Here we schematically plot the magnitude of the impedance *versus* frequency. Z_d, Z_l, Z_{di}, and Z_w refer to the impedances of the a-Si:H in the dark state, a-Si:H in the light state, dielectric, and liquid layers. For simplicity and clarity, the a-Si:H is modeled a simple resistor and the electrical double layer of the water is neglected. In order for effective switching of the voltages during illumination, the impedances of the various layers of interest must fall between the light and dark state of the a-Si:H.

In Fig. 2a, one can see there are three major frequencies f_{min}, f_c, and f_{max} which define the operating regions for OEW and OET. Below f_{min}, the impedance of the dielectric layer is larger than the dark impedance of the a-Si:H and, thus, no voltage switching can occur. Between f_{min} and f_c, and under illumination, the voltage will primarily drop across the dielectric layer (since its impedance is larger than that of the liquid layer) causing OEW to occur. Between f_c and f_{max}, and under illumination, the field now drops primarily across the liquid layer, resulting in OET. Finally, above f_{max}, the impedance of the liquid becomes so low that it drops below Z_l inhibiting effective voltage switching. With this, one can define the frequency range f_{EW} and f_{DEP}, over which OEW and OET will operate, respectively, as:

$$f_{min} < f_{EW} < f_c < f_{DEP} < f_{max} \tag{1}$$

Finally, using the simple electrical circuit model in Fig. 1a, the device dimensions/properties given in the Materials and methods section, and the standard constitutive equations for electrowetting[14] and dielectrophoresis,[15] we can then plot the normalized force as a function of frequency. The results are shown in Fig. 2b. One can clearly see a distinct peak for electrowetting (*i.e.* ideal f_{EW}) at about 10–20 kHz and one for dielectrophoresis (*i.e.* ideal f_{DEP}) an order of magnitude higher at100–200 kHz. These peaks are easily engineered simply by varying the relative thicknesses of the various device layers (*e.g.* oxide, a-Si:H, and/or liquid).

Materials and methods

Device fabrication

The device is depicted in Fig. 1a. The device consists of an ITO (300 nm) coated glass substrate, a 1 µm thick photoconductive a-Si:H layer deposited *via* PECVD (Oxford Plasmalab 80plus), a 100 nm film of Al_2O_3 deposited by ALD (Picosun Sunale R150)

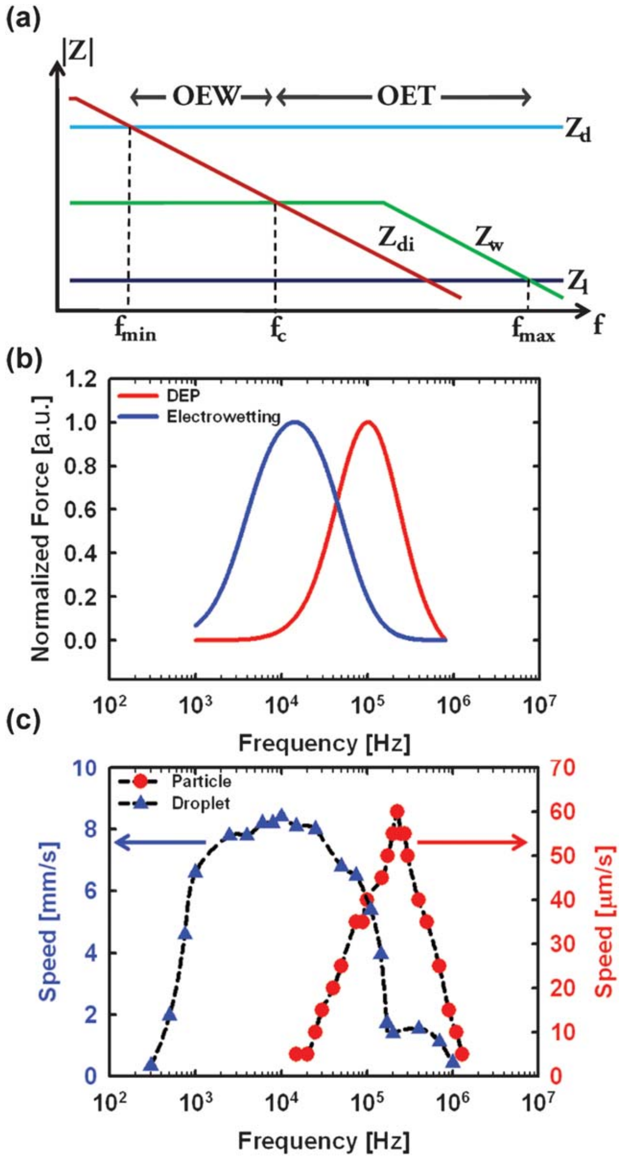

Fig. 2 (a) Graphical depiction (not to scale) of the frequency response of device showing impedance of a-Si:H in the light (Z_l) and dark (Z_d) states as well as the impedance of the liquid (Z_w) and dielectric layers (Z_{di}). OEW occurs between f_{min} and f_c, while OET occurs between f_c and f_{max}. (b) Theoretical frequency response of the normalized electrowetting force (blue) acting on a droplet and the DEP force (red) acting on an insulating bead within the droplet. OEW force is maximized at around 10–20 kHz and OET actuation is maximized at around 100–200 kHz. (c) Experimental data showing the speed (which is proportional to force) of a 12.5 nL droplet (blue, 40 Vppk (volts peak-to-peak)) and the speed of a 10 µm polystyrene bead (red, 10 Vppk). The droplet movement is maximized at 10 kHz due to electrowetting, though a secondary hump is present at 200 kHz due to DEP enhancement of the droplet movement. Bead speed is maximized at 200 kHz due to DEP.

and a 25 nm film of spin coated 0.2% Teflon (3000 rpm, 30 s). The top substrate is formed from another Teflon-coated ITO glass wafer. The entire fabrication process does not require any photolithographic steps. The two substrates are then placed on top of one another separated by a spacer layer of double-sided tape (100 µm) forming the microfluidic manipulation chamber.

Sample preparation

Samples are prepared by suspending 10 µm fluorescent polystyrene beads (Polysciences Inc.) or HeLa cells in a 10 mS m^{-1} isotonic aqueous solution along with 0.2% Pluronic F-68 surfactant (Sigma Aldrich). Droplets of the polystyrene or cell mixture are then deposited on the device and surrounded by silicone oil (1.0 cSt trimethylsiloxy-terminated polydimethylsiloxane, Gelest Inc.).

Experimental setup

Device bias is applied between the two ITO layers (10–40 Vppk (volts peak-to-peak), 1–500 kHz (Agilent 33220A)). Optical patterns are generated by a commercial data projector (Dell 4210X) controlled by an external computer and focused onto the device using a 1 : 1 telescope. Viewing occurs through a continuous zoom lens system (Navitar 12×) connected to a CCD camera (Sony XCD-X710CR). Fluorescent illumination (EXFO, XCite 120) along with appropriate filters (Chroma Technology) is also integrated into the optical train to enhance viewing of the polystyrene beads. Speed measurements for the polystyrene beads and cells are extracted using a motorized stage controller (Newport ESP300).

Results and discussion

Speed *vs.* frequency characterization

In order to experimentally determine the effective operating regimes of the device, a 12.5 nL, 10 mS m^{-1} aqueous droplet containing 10 µm polystyrene beads was placed in the device and the droplet's resulting maximum speed was measured as a function of frequency at 40 Vppk. Next, the speed of a 10 µm polystyrene bead (while the droplet remained stationary) was measured as a function of frequency at 10 Vppk. The resulting speeds are depicted in Fig. 2c. One can see that the droplet speed peaks at 8 mm s^{-1} at around 10 kHz and the bead speed peaks around 200 kHz at 60 µm s^{-1}. These results agree well with the predictions of Fig. 2b.

Also, it is interesting to note the additional bump in droplet speed at 200 kHz. This is likely due to DEP enhancement of the droplet movement (*i.e.* liquid dielectrophoresis[16]) which peaks at this same frequency (as indicated by the particle speed). It is important to note that even at 200 kHz, where the particle speed is at a maximum, the droplet can still be moved (albeit slowly). This movement is likely unwanted as the droplet movement will affect the particle placement and movement. This can be prevented by selecting a light pattern that is small relative to the droplet (but still large enough to move the particles of interest), thus preventing droplet movement. Additionally, using a lower voltage for particle manipulation compared to that used for droplet movement will prevent unwanted droplet translation.

Particle concentration

One potential application/benefit of having an integrated platform for droplet and particle manipulation is the ability to perform on-chip sample concentration/purification. This process is depicted in Fig. 3a. Here, particles are concentrated towards

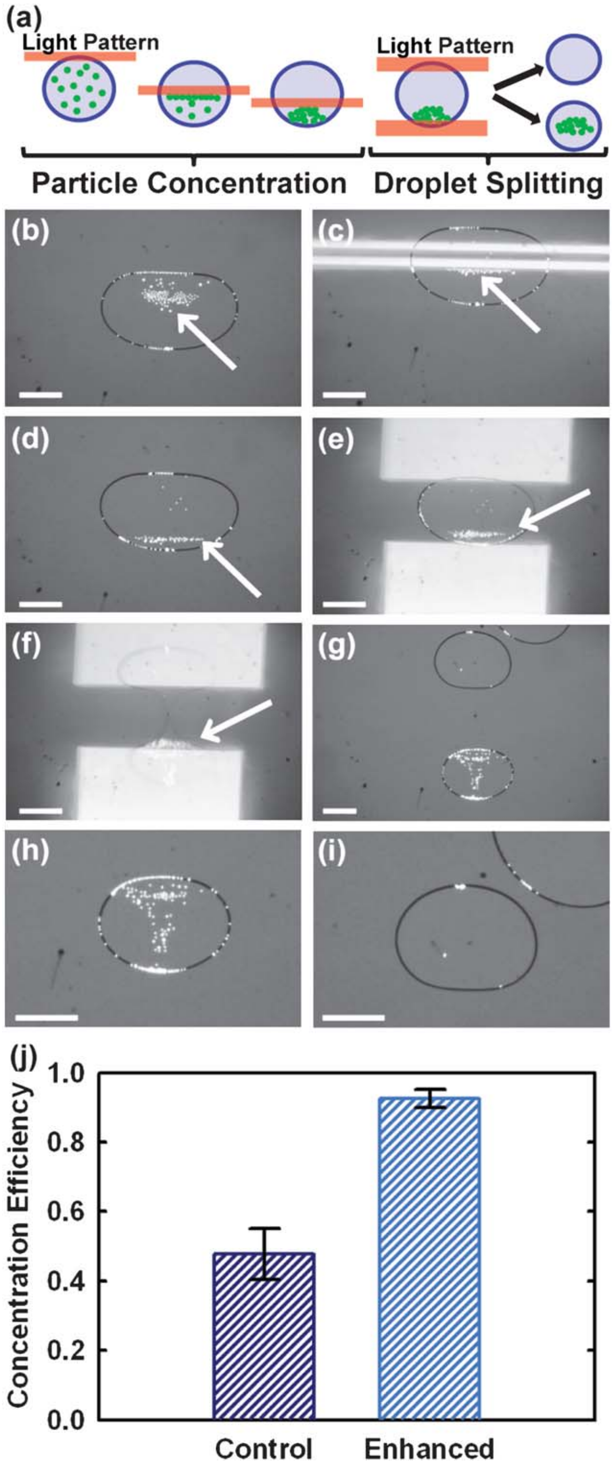

Fig. 3 (a) Method of particle concentration. (b–i) Experimental demonstration of particle concentration. A 335 nL droplet containing fluorescent polystyrene beads (white arrow) is placed in the device (b). A light pattern is swept across the device (c) (16 Vppk, 200 kHz) resulting in OET on the beads and causing a concentration of beads at one end of the droplet (d). Next the droplet is split (e–g) using OEW (32 Vppk, 10 kHz) resulting in a concentrated (h) and diluted (i) droplet. Scale bar 750 μm. (j) Plot of the concentration efficiency for a control group (without OET) and an enhanced group (with OET). The enhanced group average efficiency is 93%.

one end of the droplet using OET. Next, the droplet is split using OEW into two droplets, one containing the concentrated particles while the other remains empty. In this manner, the concentration/purity is effectively doubled.

Fig. 3b–i show video frames of this process (also see Video S1, ESI†). Fluorescent, polystyrene beads are suspended in a 335 nL, 10 mS m^{-1} aqueous buffer. A light pattern is then swept across the droplet at 16 Vppk, 200 kHz and the beads are pushed (*via* negative DEP) towards the bottom of the droplet. Next, two light patterns are positioned at the top and bottom of the droplet and a 32 Vppk, 10 kHz bias is applied. This causes the droplet to split into two resulting in a concentrated droplet (Fig. 3h) and a diluted droplet (Fig. 3i).

As a means of quantitatively measuring the effectiveness of the concentration process a concentration efficiency is typically defined as:[5]

$$\text{Efficiency} = \frac{\#\ \text{of beads in concentrated droplet}}{\#\ \text{of beads in original droplet}} \quad (2)$$

Fig. 3j shows a comparison of the efficiency factors for a control group (without OET pre-concentration) and an enhanced group (with OET pre-concentration). The control group efficiency is, unsurprisingly, about 50% while the enhanced group shows an average efficiency of 93%. The remaining 7% of beads not remaining in the concentrated droplet are typically either adhered to the surface or oil–water interface and prevent efficient movement during OET pre-concentration.

It should be noted that the times required for this process are fairly slow (minutes). The constraining factor here is the rate at which the particles can be concentrated to one end of the droplet. In the case presented here, the 10 μm beads must be displaced a maximum of 2 mm (diameter of 335 nL droplet). So, at a nominal particle speed of 10 μm s^{-1} (Fig. 2c), this requires more than 3 minutes. Of course, this speed can be increased by applying larger voltages, however, as discussed earlier, too large a voltage results in droplet movement as well (due to DEP of the droplet itself), which is undesirable. More realistically, the speed can be increased by increasing the optical power density on the substrate. This, in effect, creates more carriers in the a-Si:H layer and subsequently increases the field gradients per DEP force seen by the particles. In these experiments, an optical power density of <1 W cm^{-2} is used. By using a higher powered projector or a more sensitive photoactive layer (*e.g.* phototransistor), electric field gradients can be easily increased, resulting in higher actuation speeds (∼100 μm s^{-1}). With this increase in speed, the concentration steps can be brought down into the 10s of seconds.

This technique could serve as an alternative to magnetic bead purification.[17] Except in this case, various types of beads (with varying electrical and, thus, DEP responses) could be functionalized. Then using the varying DEP responses, the beads with one functionalization could be sorted from others resulting in a simultaneous and/or selective purification strategy.

Serial particle concentration

A feature of this platform that is difficult to reproduce with standard microelectrode-based devices is the ability to perform serial particle concentration. This process is depicted in Fig. 4a. Here, like in Fig. 3a, particles are concentrated towards one end of

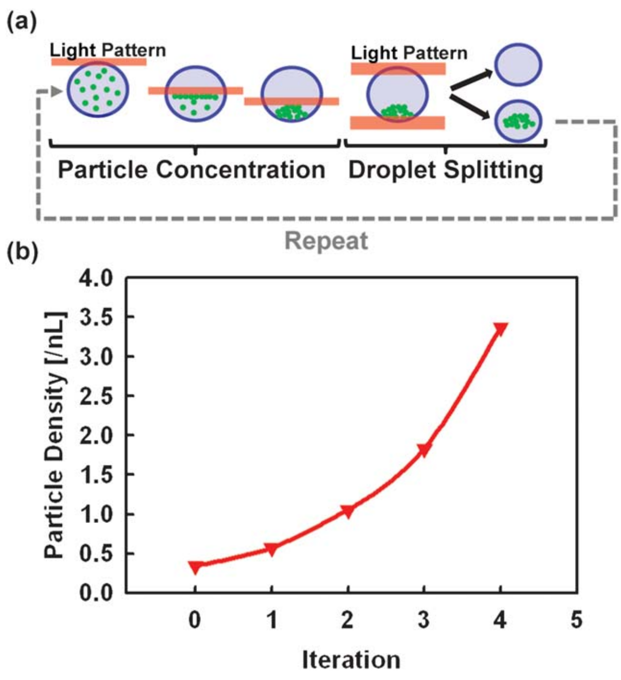

Fig. 4 (a) Method of serial particle concentration. (b) Particle density as a function of the number of times the particle concentration process of Fig. 3a has been performed. The particle density increases exponentially as a function of the iteration number. The final particle density is 10× the original.

the droplet and the droplet is split into a concentrated and diluted droplets. However, now one takes the concentrated droplet and repeats the process serially. Since the effective volume is reduced in half each time, the concentration will double each time resulting in an exponential increase in particle concentration as a function of the number of iterative concentrations performed. Fig. 4b shows the exponential increase in particle concentration for 4 iterations, resulting in a 10× concentration enhancement relative to the starting value. This process typically can continue until the resulting droplets are too small to split using OEW. This is generally dictated by the aspect ratio (droplet diameter : droplet height) of the droplet. Typically, the minimum aspect ratio at which a droplet can still be reliably split with this technique is 4 : 1.

The reason this is difficult to perform with existing techniques is that the lithographically defined electrode size determines the minimum droplet that can be manipulated/split. Therefore, since the droplet size is halved each time in this process, a large number of individually addressable electrodes are required resulting in relatively complex fabrication and addressing schemes. In this case, however, the electrode is determined by the size of the light pattern, and, therefore, smaller and smaller light patterns can be projected to account for the varying droplet diameters. Of course, the minimum projected light pattern is limited as well, and this will be the smaller of either the diffraction limit of the projected light or the diffusion length of the photoconductive material (both are typically on the order of 100 nm).

Single cell selection and encapsulation

The ability to encapsulate single cells in micro-scale droplets is of great interest for those interested in fields such as single cell analysis and/or sorting. Traditionally, this process relies on a statistical approach which ensures that some percentage of generated droplets contain single cells and does not afford the ability to select individual cells from a population for encapsulation.[18,19] However, work using optical tweezers has achieved the ability to encapsulate individual cells selectively.[20] But, the large optical power necessitated by optical tweezers is often detrimental to living structures.[21] Since the technique presented here requires far less optical power (~10^5×),[13] cells are far less susceptible to damage.

Fig. 5 demonstrates the ability to select an individual HeLa cell from a cohort and then encapsulate it (also see Video S2, ESI†). The process is depicted in Fig. 5b–g where an individual HeLa cell is selected from a group of three. The selected cell is moved *via* OET (16 Vppk, 10 kHz) to one end of the droplet while the other two cells are moved towards the other end of the droplet. Note that under these conditions, the cells experience a positive DEP force here as compared to the negative DEP force experienced by the polystyrene beads. Then the droplet is split using OEW (32 Vppk, 200 kHz) resulting in one 75 nL droplet containing the selected cell (Fig. 5f) and one 75 nL droplet containing the remaining two cells (Fig. 5g). This demonstrates the ability to perform single particle manipulation continuously over the entire surface of the device and then, subsequently, encapsulate that particle. Once again, this would be very difficult to implement with non-optically-based techniques

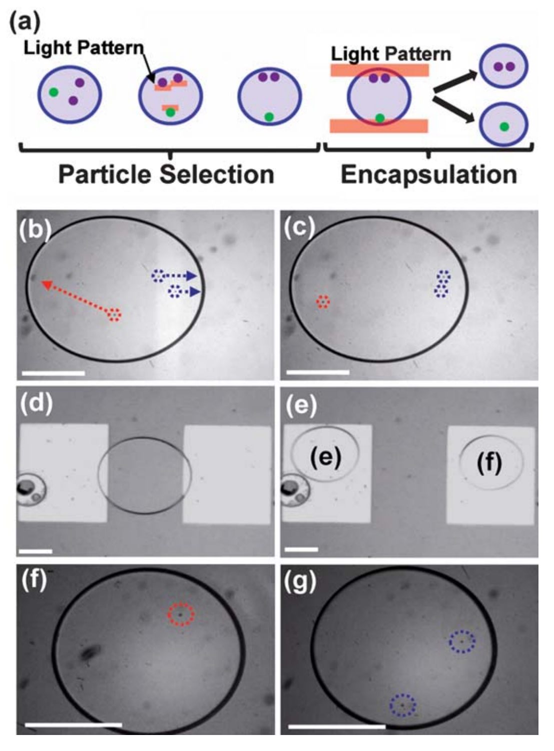

Fig. 5 (a) Method of single cell selection and encapsulation. (b and c) A group of three HeLa cells exist within a 150 nL droplet. One cell is selected (red) and moved towards one side of the droplet while the other two (blue) are moved towards the opposite side (16 Vppk, 200 kHz). (d and e) Next, the droplet is split with OEW into two 75 nL droplets (36 Vppk, 10 kHz). The resulting droplets contain the single cell of interest (f) and the remaining two cells (g). Scale bar 500 μm.

(*i.e.* microelectrode-based) as a large number of individually addressed electrodes would be necessary to insure single particle control.

It should be briefly mentioned that during DEP manipulation the cells are subjected to a non-zero electric field (<0.8 kV cm^{-1} in this case). This can presumably lead to unwanted cell perturbations. However, we have previously shown that cell viability is maintained under these conditions indicating that the electric field effects, in this case, are negligible.[22] Additionally, the cells are placed in an isotonic buffer that has a substantially lower ($\sim$100$\times$) conductivity than that of culture media. This constrains the time the cells can be manipulated to a couple of hours while maintaining cell viability. This low conductivity buffer is required since the device will only operate over a certain range of liquid conductivities that is fundamentally controlled by the light and dark conductivities of the a-Si:H layer. We have recently developed a device capable of operating in cell culture media using a phototransistor-based structure.[23] In the future, this device can be integrated with the existing droplet manipulation platform to allow for cell manipulation in a native environment.

Conclusions

A unified platform for on-chip particle and droplet manipulation is introduced. The technique uses optoelectrowetting and optoelectronic tweezers as the manipulation modalities. Switching between droplet and particle manipulation is achieved through a change in the externally applied electrical frequency. The device allows for the continuous manipulation of both droplets and particles over its surface by eliminating the need for lithographically patterned microelectrodes. As such, the fabrication process is much simplified and requires no photolithography. Finally, the use of light to pattern the electrodes enables full 2-dimensional single particle control.

Droplet and 10 μm particle speeds of up to 8 mm s^{-1} and 60 μm s^{-1} are achieved under modest bias conditions. The ability to perform particle/sample concentration with efficiencies of 93% as well as the ability to repeat this process serially result in an exponentially increasing particle density and a 10$\times$ concentration enhancement. Finally, the ability to effect single cell selection and encapsulation is demonstrated.

The development of a device that allows for a seamless integration of both droplet and particle manipulation that is simultaneously low-cost, high-resolution, and reconfigurable may one day form a foundation for a multitude of applications in both biology and chemistry.

Acknowledgements

The authors would like to thank the UC Berkeley Cell Culture facility for providing the cells used in this study and the UC Berkeley Microlab where all devices were fabricated. This work was funded by the Center for Cell Control, a National Institutes of Health Nanomedicine Development Center, under grant #PN2 EY018228.

References

1 H. Becker, *Lab Chip*, 2009, **9**, 2119–2122.
2 S. K. Cho, H. J. Moon and C. J. Kim, *J. Microelectromech. Syst.*, 2003, **12**, 70–80.
3 F. Mugele and J. C. Baret, *J. Phys.: Condens. Matter*, 2005, **17**, R705–R774.
4 A. R. Wheeler, *Science*, 2008, **322**, 539–540.
5 S. K. Cho, Y. J. Zhao and C. J. Kim, *Lab Chip*, 2007, **7**, 490–498.
6 W. Yizhong, et al., *J. Micromech. Microeng.*, 2007, **17**, 2148.
7 S.-K. Fan, P.-W. Huang, T.-T. Wang and Y.-H. Peng, *Lab Chip*, 2008, **8**, 1325–1331.
8 Y. Zhao, U.-C. Yi and S. K. Cho, *J. Microelectromech. Syst.*, 2007, **16**, 1472–1481.
9 G. J. Shah, A. T. Ohta, P. Y. Chiou, M. C. Wu and C.-J. Kim, *Lab Chip*, 2009, **9**, 1732–1739.
10 P. Y. Chiou, S.-Y. Park and M. C. Wu, *Appl. Phys. Lett.*, 2008, **93**, 221110.
11 S. N. Pei, J. K. Valley, S. L. Neale, A. Jamshidi, H.-Y. Hsu and M. C. Wu, *Micro Electro Mechanical Systems (MEMS), 2010 IEEE 23rd International Conference*, 2010, **23**, 252–255.
12 P. Y. Chiou, H. Moon, H. Toshiyoshi, C. J. Kim and M. C. Wu, *Sens. Actuators, A*, 2003, **104**, 222–228.
13 P. Y. Chiou, A. T. Ohta and M. C. Wu, *Nature*, 2005, **436**, 370–372.
14 V. Bahadur and S. V. Garimella, *J. Micromech. Microeng.*, 2006, **16**, 1494–1503.
15 T. B. Jones, *Electromechanics of Particles*, Cambridge University Press, Cambridge, 1995.
16 T. B. Jones, *Langmuir*, 2002, **18**, 4437–4443.
17 M. A. M. Gijs, *Microfluid. Nanofluid.*, 2004, **1**, 22–40.
18 S. Koster, F. E. Angile, H. Duan, J. J. Agresti, A. Wintner, C. Schmitz, A. C. Rowat, C. A. Merten, D. Pisignano, A. D. Griffiths and D. A. Weitz, *Lab Chip*, 2008, **8**, 1110–1115.
19 J. F. Edd, D. Di Carlo, K. J. Humphry, S. Koster, D. Irimia, D. A. Weitz and M. Toner, *Lab Chip*, 2008, **8**, 1262–1264.
20 M. He, J. S. Edgar, G. D. M. Jeffries, R. M. Lorenz, J. P. Shelby and D. T. Chiu, *Anal. Chem.*, 2005, **77**, 1539–1544.
21 K. C. Neuman, E. H. Chadd, G. F. Liou, K. Bergman and S. M. Block, *Biophys. J.*, 1999, **77**, 2856–2863.
22 J. K. Valley, S. Neale, H.-Y. Hsu, A. T. Ohta, A. Jamshidi and M. C. Wu, *Lab Chip*, 2009, **9**, 1714–1720.
23 H.-Y. Hsu, A. T. Ohta, P.-Y. Chiou, A. Jamshidi, S. L. Neale and M. C. Wu, *Lab Chip*, 2010, **10**, 165–172.

